6

Adaptive Radar System to Visualize Antipersonnel Plastic Landmines

We extend the idea in the adaptive classification described in Chapter 5 by introducing frequency-domain information to visualize plastic landmines buried shallowly underground. Antipersonnel landmines, in particular plastic ones, use so slight metal that it is difficult to detect them with metal detectors because many shots and metal fragments are scattered under battlefields. The shallowness also causes serious surface-reflection noise. We construct a phase-sensitive millimeter-wave / microwave front-end to observe ground reflection in spatial and frequency domains, and feed the data to a complex-valued self-organizing map (CSOM). The CSOM visualizes plastic landmines by segmenting the reflection image adaptively.

6.1 Ground Penetrating Radars

Ground penetrating radars (GPRs) are widely used in many fields such as buried-object detection, ruin explorations, and groundwater surveillance. In landmine detection, we also expect to apply them to nonmetal landmine detections, and many researches have been done in a long while. However, the detection of antipersonnel plastic landmines is mostly still difficult in practice because of the small target size, low reflectance, and relatively large land-surface reflection when they are buried shallowly underground. At the same time, insufficiency of demining professionals and high danger of operation augments the demand for support and automatization of the demining operation.

The complex-valued self-organizing map (CSOM) is highly effective in such a task. When a part of electromagnetic wave penetrates ground surface and landmine itself, we want to measure the range distribution (and texture) of reflectance. Then, by applying the CSOM to processing data obtained at multiple frequencies, we can expect a successful adaptive segmentation of three-dimensional data, i.e., in the propagation direction and the transversal two-dimensional space. Because the inverse Fourier transform of the

A. Hirose: Complex-Valued Neural Networks, SCI 400, pp. 113–122.
springerlink.com

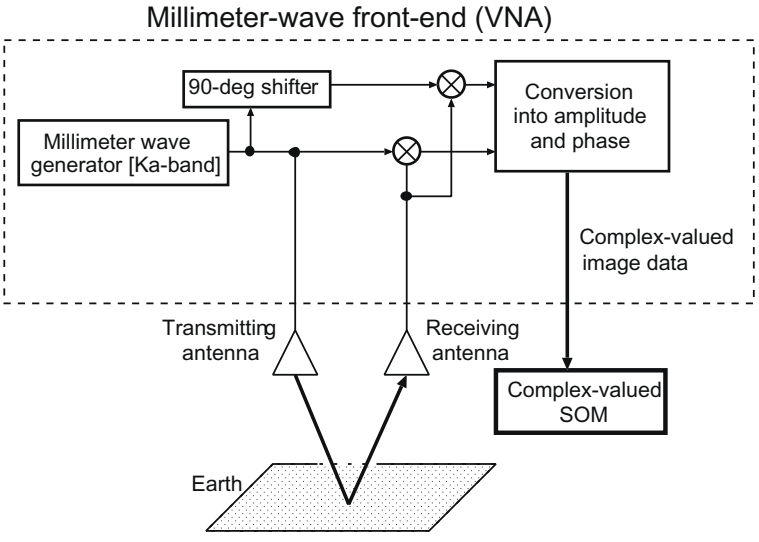

Fig. 6.1 Adaptive plastic-landmine visualization system consisting of millimeter-wave / microwave antennas, front-end, and CSOM processing unit [149][2].

frequency-domain data gives the time-domain reflection of an electromagnetic-wave pulse, the above processing is equivalent to classification of reflection texture in three dimensions.

In the system presented in this chapter, we observe the amplitude and phase of reflection at multiple frequencies to acquire complex-amplitude images. We visualize landmines adaptively by classifying the reflection texture in three dimensions, i.e., frequency + two-dimensional-space dimensions, by utilizing frequency-domain information in the CSOM [199] [149] . We also compare the result obtained by the CSOM with that by a conventional real-valued SOM dealing with amplitude texture only.

6.2 Construction of CSOM Plastic Landmine Visualization System Dealing with Frequency- and Space-Domain Texture

Figure 6.1 shows the schematic construction of the system focusing on the antennas and the front-end. A vector network analyzer (VNA) is used for

[2]Figs.6.1, 6.3, 6.4, 6.5 and Table 6.1 are reprinted from [149]: *Neural Networks*, vol.17, No.8–9, Takahiro Hara and Akira Hirose, "Plastic mine detecting radar system using complex-valued self-organizing map that deals with multiple-frequency interferometric images," pp.1201–1210, Copyright (2004), with permission from Elsevier. Japanese review [200] is also helpful for further understanding of the background and the technology.

homodyne detection of the received reflection. We obtain the amplitude and phase information simultaneously. The transmitter and receiver are rectangular horn antennas. The frequency range is 30−40GHz. The wider the frequency bandwidth is (which requires a higher center frequency), the higher resolution we can enjoy. However, a too high frequency is not suitable for GPRs because it will be so largely absorbed by the soil that we cannot see underground. We prepare a 70×70cm corrugated-cardboard box with a thin plastic sheet paved inside, and put ordinary Tokyo soil, containing stones and miscellaneous, and a target object in it. We move the pair of antennas facing to the soil horizontally, and obtain complex-valued data at multiple frequency points. The system is totally controlled by a personal computer (PC), and the obtained data is stored also in the PC, where the CSOM classifies pixels in the images by conducting the adaptive segmentation.

6.3 Adaptive Signal Processing in CSOM

As described in the previous chapter, first we prepare a small window block at around a pixel we focus on. In the block, we generate a feature vector reflecting the stochastic properties contained in the pixel values (texture). We sweep the whole image with the block, calculating a feature vector in the block at each position. Then we classify the obtained feature vectors adaptively in the CSOM in such a manner that the classification reflects the feature-vector distribution in the information space. Finally, we segment the image by labeling each pixel with the class into which the block belongs.

In this system, we observe reflection at multiple frequency points. The Fourier-transform operation reveals that the frequency-domain data contains information essentially identical to that of the time-domain data, i.e., the depth-direction reflection information. It is possible that, first, we Fourier transform the frequency-domain data inversely into time-domain one. In the present adaptive system, however, we deal with the frequency-domain data directly without the linear transform as follows.

6.3.1 Feature Vector Extraction by Paying Attention to Frequency Domain Information

Figure 6.2 shows the construction of the adaptive three-dimensional radar-image segmentation system consisting of two modules, namely, a complex-valued feature extractor and a CSOM in its narrow sense. We prepare a window block having a size of $L \times L$ on a set of input images measured at N_f frequency points. The feature extractor calculates a feature vector expressing stochastic properties of the pixel values in the block. As we did in the previous chapter, we adopt the complex-valued mean and covariances as the feature vector elements. We shift the block pixel by pixel, and calculate a local feature vector for the block at each position. Finally, the block finishes sweeping the

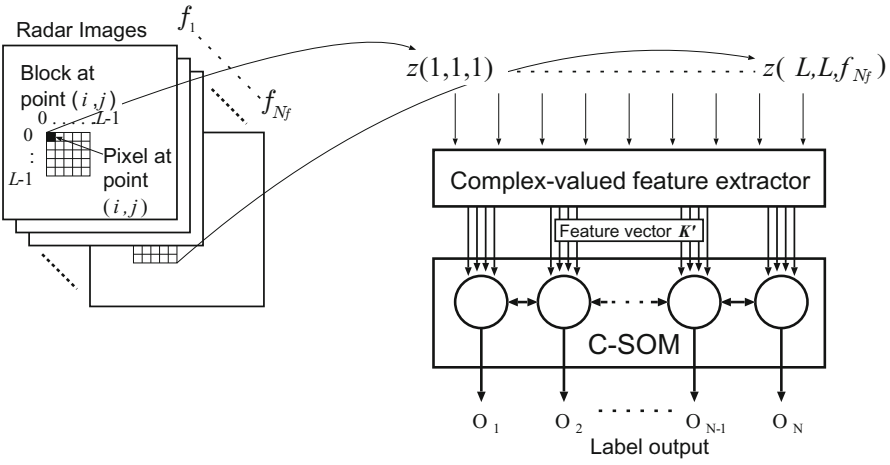

Fig. 6.2 Construction of the adaptive three-dimensional radar-image segmentation system [201][4].

whole image set. We feed the feature vectors sequentially to the CSOM, which determines adaptively which class each vector should belong to.

The procedure is described as follows. We consider the mean M and the covariances $K(\xi, \eta, f_\zeta)$ in each block as the elements of the feature vector $\boldsymbol{K}$. We determine the mean M and a covariance K in an $L \times L$ block for complex-valued pixel data $z(i, j, f)$ as

$$M = \frac{1}{L^2} \sum_{i=0}^{L-1} \sum_{j=0}^{L-1} z(i, j, f_\mathrm{b}) \tag{6.1}$$

$$K(\xi, \eta, f_\zeta) = \frac{1}{L^2} \sum_{i=0}^{L-1} \sum_{j=0}^{L-1} z(i, j, f_\mathrm{b})\ z^*(i + \xi, j + \eta, f_\mathrm{b} + f_\zeta) \tag{6.2}$$

where f_b is a basis frequency determined arbitrary.

The total number of the covariances $K(\xi, \eta, f_\zeta)$ is enormous because of the possible combinations of the variables ξ, η, and f_ζ. To avoid this explosive expansion, we consider approximately that the spatial- and frequency-domain data are qualitatively orthogonal to each other. Then, the covariance elements have two parts, namely, the covariances in spatial domain $\boldsymbol{K}_s$ at a basis frequency f_b, and those in frequency domain $\boldsymbol{K}_f$. Finally, we take into account only the four spatial-domain values (mean M, variance $K(0, 0, 0)$

[4]Fig.6.2 is reprinted from [201]: *System and Human Science – For Safety, Security and Dependability* (T.Arai, S.Yamamoto, K.Makino (eds.)), Akira Hirose and Takahiro Hara, "Complex-valued self-organizing map: A framework of adaptive processing for multiple-frequency millimeter-wave interferometric imaging systems," pp.299–308, Copyright (2004), with permission from Elsevier.

(i.e., energy), covariances $K(0,1,0)$, $K(1,0,0)$, and $K(1,1,0)$) and a limited number of frequency-domain ones (covariances $K(0,0,f_\zeta)$). That is,

$$\boldsymbol{K} \equiv [\boldsymbol{K}_s, \boldsymbol{K}_f] \tag{6.3}$$

$$\boldsymbol{K}_s \equiv [M, K(0,0,0), K(0,1,0), K(1,0,0), K(1,1,0)] \tag{6.4}$$

$$\boldsymbol{K}_f \equiv [K(0,0,f_1), K(0,0,f_2), \cdots, K(0,0,f_{N_f})] \tag{6.5}$$

In (6.4) and (6.5), $K(0,0,0)$ is always a real number, while others are complex numbers.

With this feature vector, we expect qualitatively an adaptive segmentation of the image as follows. First, we consider the relationship in the pixel values in the frequency domain. If, at a local spot or a point, the soil including objects has some specific reflection at certain depths differently from its surrounding area, the frequency-domain-correlation elements are expected to express certain values specific to the frequency-domain texture at the point. The peculiarity assigns the feature vector $\boldsymbol{K}$ to a special location in the feature-vector information space. Then the points containing the identical feature are clustered in a single class.

Next, we consider the pixel-value relationship in the spatial domain. Remember the process described in Chapter 5 (clustering Mount Fuji, etc.). When we *see* the phase image, we regard the mountain as a mass. We deal with only the steepness of slopes without slope directions. Such treatment probably works well also in the present landmine visualization. Therefore, we adopt a direction-insensitive slope variables as we did in Chapter 5 . When we write the spatial feature-vector elements $K(\xi,\eta,0) \in \boldsymbol{K}_s$ in polar coordinate as

$$K(\xi,\eta,0) = |K(\xi,\eta,0)|\, e^{j\varphi(\xi,\eta,0)} \tag{6.6}$$

the phase value φ in (6.6) represents the slope information. Therefore, we modify K_s to adopt a new one as

$$K'(\xi,\eta,0) = |K(\xi,\eta,0)|\, e^{j|\varphi(\xi,\eta,0)|} \tag{6.7}$$

By using the K'_s, we define a new feature vector $\boldsymbol{K}'$ as

$$\boldsymbol{K}' \equiv [\boldsymbol{K}'_s, \boldsymbol{K}_f] \tag{6.8}$$

We use $\boldsymbol{K}'$ as the feature vector to be fed into the CSOM.

6.3.2 Dynamics of CSOM Classification

The CSOM classifies the feature vectors according to the dynamics described in Chapter 4. In the present case, we assign a window block to every pixel position, and calculate the statistic features in the block to determine the

feature vector $\boldsymbol{K}'$. The number of the vectors fed to the CSOM is the pixel number in total (see Section 4.5). The CSOM classifies the vector determined for every pixel position into a class adaptively. By coloring the pixel according to the class into which the vector is classified, the set of the input images for an observation is segmented in the manner that reflects the result of the adaptive classification. Then we find spatial clusters in the segmented images.

In buried-object detection like the present case, the depth information plays a significantly important role. Though a pulse-radar system usually possesses depth information in the time-domain data, the multiple-frequency continuous-wave (CW) interferometric radar system has this information in the frequency-domain data. The Fourier transform reveals substantial equivalence between the frequency-domain data and the time-domain one. In our system, however, we do not employ the Fourier transform, which is a linear processing, but, instead, apply the nonlinear and adaptive CSOM processing directly to the frequency-domain feature-vector information. In this process, we expect the follows. We have a plastic object having a certain thickness at a certain depth. Then we observe specific signals such as frequency-dependent characteristic reflection and resonance. Such signals make the feature vector distribution inhomogeneous and, instead, specific to the object in the feature-vector space. The CSOM segments the distribution into a number of classes adaptively.

6.4 Visualization of Antipersonnel Plastic Landmines

6.4.1 Measurement Parameters

As shown in Fig.6.1, we place antennas facing to the land surface. We bury a mock plastic landmine called TYPE 72 whose diameter and height are 78mm and 40mm, respectively. It is filled with a substance having the same permittivity as that of explosive. Parameters in electromagnetic-wave observation and CSOM processing are shown in Table 6.1.

Table 6.1 Parameters in measurement and CSOM processing [149].

Start frequency	$f_{\min}$	30.0GHz
Stop frequency	$f_{\max}$	40.0GHz
Frequency point number	N_f	81
Frequency interval	Δf	125MHz
Scanning area	$X \times Y$	381.0mm × 381.0mm
Sampling point number	$N_x \times N_y$	128 × 128
Sampling interval	ΔX (ΔY)	3.0mm
Clustering class number	$s_{\max}$	16

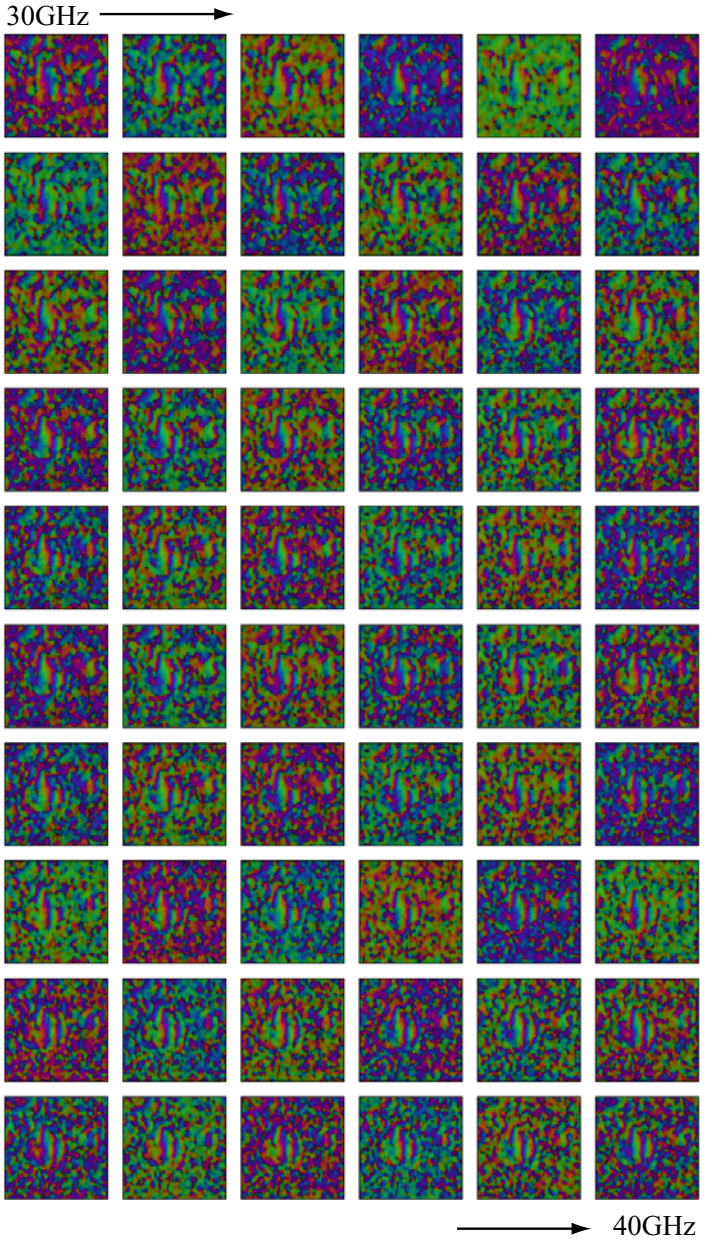

Fig. 6.3 Complex-amplitude images obtained in multiple-frequency observation of a plastic landmine buried shallowly underground where brightness shows intensity and hue shows phase [149].

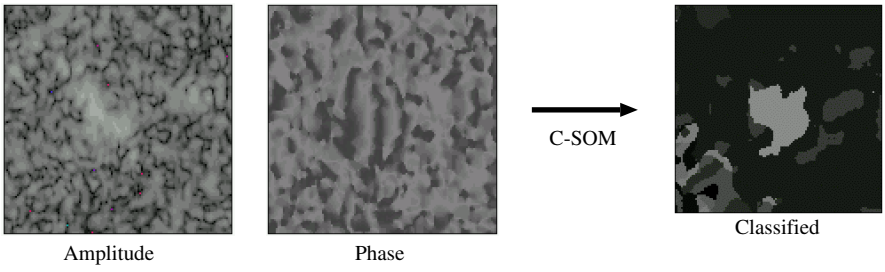

Fig. 6.4 Adaptive visualization result for a plastic landmine buried shallowly underground [149].

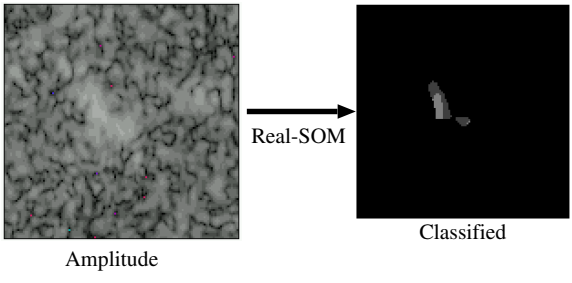

Fig. 6.5 Adaptive visualization result for a plastic landmine buried shallowly underground with a conventional (real-valued) SOM [149].

6.4.2 Results of Observation and Classification

First, we examine the raw data obtained in the observation. Figure 6.3 shows the phase images in grayscale observed at multiple frequency points for the mock plastic landmine buried shallowly underground at about 1cm depth. Black corresponds to $-\pi$ phase angle, while white means π. The frequency is 30GHz in the top-left image, whereas it is 40GHz in the bottom-right one, and the frequency is changed stepwise with a constant interval. When we see each image individually, we cannot find anything hidden. That is, even human brain cannot detect a landmine.

Actually, a round plastic landmine is buried at the center. When we know this fact, and when we examine all the images in total, not a few readers probably find that we can construct something round intuitively in our mind. With our volition, we can *see* something undetected when we watch a single image. However, we have still difficulty in *seeing* it.

If we analyze our mind, we may say the follows. First, the central area presents more-orderly changes in the space than the surrounding areas. The soil-and-stone areas have more random phase changes. In the frequency domain, we can also find more-orderly changes in the central area, though the

frequency-domain changes are little more difficult to notice. The role of the CSOM is to extract such differences in the texture to visualize the object.

In contrast, the amplitude images observed at multiple-frequency points are similar to each other. As an example, we show an amplitude image on the left-hand side in Fig.6.4 in grayscale. White means a high power, while black means a low one. In Fig.6.4, the next image is the phase image. We can find in the amplitude image that the power is a little high at the center. However, the shape is not round. Moreover, in multiple observations, we find similar high-power reflection even for a buried metal bolt. Therefore, it is difficult to find plastic landmines only with the amplitude observation.

The right-hand-side image in Fig.6.4 is the result of the CSOM segmentation. We clearly find something round at the center. The CSOM system visualizes the plastic landmine buried shallowly underground by performing an effective segmentation in the observed images successfully.

On the other hand, Fig.6.5 shows a result when we employ a conventional (real-valued) SOM for segmentation of the amplitude image. Though we can find something small at the center, the visualization quality is much lower than that of the CSOM in comparison with the result in Fig.6.4. We cannot say that the landmine area is segmented with the conventional SOM.

The comparison between the results of the real-valued SOM and the CSOM, we find that the round shape of the landmine has been brought about by the phase information. That is to say, the CSOM has successfully performed the segmentation that we could do, in Fig.6.3, when we examine the spatial and frequency-domain phase data in total, and when we know the correct answer. The CSOM has worked as a phase-sensitive superbrain.

6.4.3 Performance Evaluation by Visualization Rate

We repeated experiments to estimate the success rate in visualization. With our present CSOM system, the rate is about 70%, while it is about 10% for a real-valued SOM, which suggests the effectiveness of the CSOM processing. The value of 70% is comparable to the rate that a metal detector finds metal landmines. In this sense, at least, the present system has a sufficient ability in practical use.

6.5 Summary

In this chapter, we have presented a CSOM system to visualize plastic landmines buried shallowly underground by dealing with complex-amplitude images obtained at multiple-frequency points. By comparing the result with that of a real-valued SOM, we have discussed in what way the CSOM realizes a successful visualization.

It is urgent to detect and remove plastic landmines in the world. Needless to say, we have to develop useful techniques to realize efficient detections

of plastic landmines. Complex-valued neural networks provide the human beings with solutions in such problems.

In the first decade of 2000s, the system presented here has been modified and improved into a series of small portable visualization systems employing array antennas for quick acquisition of scattering / reflection of electromagnetic wave. They have been tested in the field of Cambodia, for example, for further improvement for practical use in the near future [151] [152] [154].

The neural processing in two-dimensional space $\times$ frequency-domain (or time-domain) data realizes an adaptive processing of three-dimensional spatial information. The importance of such three-dimensional adaptive processing will increase more and more in many fields related to millimeter wave and microwave systems such as intelligent transport systems (ITS) and multiple-input multiple-output (MIMO) systems where we use multiple antennas in transmission and detection in wireless communications.